Bol. Soc. Paran. Mat.
©SPM – E-ISSN-2175-1188
SPM: www.spm.uem.br/bspm

(3s.) **v. 2026 (44) 2** : 1–13.
ISSN-0037-8712
doi:10.5269/bspm.80518

Unsteady Rotating MHD Jeffreys Fluid Flow with Thermal Radiation and Chemical Reaction Effects

Mantha Srikanth, M. Harikrushna, G. Balreddy and K. Madhusudhan Reddy

ABSTRACT: This study examines the unsteady magnetohydrodynamic (MHD) flow of a Jeffreys fluid in a rotating porous medium, incorporating thermal radiation, chemical reaction and buoyancy effects. The governing momentum, energy and mass equations are developed and analytically solved using the Laplace transform. The impacts of key dimensionless parameters—magnetic field (M), permeability (K), rotation (Ω), thermal and solutal Grashof numbers (Gr, G_m), Prandtl number (Pr), Schmidt number (Sc) and reaction parameter (γ)—on velocity, temperature and concentration profiles are analyzed. Results show that magnetic effects reduce fluid velocity due to the Lorentz force, while rotation modifies both primary and secondary velocities. Buoyancy forces increase convective strength, and thermal radiation elevates temperature levels, particularly at higher Prandtl numbers. Concentration gradients become steeper with increasing Schmidt number and reaction rate. Engineering parameters, including skin friction, Nusselt number and Sherwood number, are evaluated, indicating a decrease in skin friction with stronger magnetic fields.

Keywords: Magnetohydrodynamics, Jeffreys fluid, thermal radiation, chemical reaction, buoyancy forces, porous medium, Laplace transform.

Contents

2020 *Mathematics Subject Classification:* 35B40, 35L70.
Submitted November 30, 2025. Published March 14, 2026

1. Introduction

Fluid dynamics has consistently been a cornerstone of applied mathematics, engineering, and physics. The study of non-Newtonian fluids has gained considerable attention due to their wide industrial and biomedical applications. Among these, the Jeffreys fluid model provides a classical representation of viscoelastic behaviour, exhibiting both elastic and viscous characteristics. This work examines the unsteady magnetohydrodynamic (MHD) flow of an electrically conducting, incompressible Jeffreys fluid in a rotating system embedded in a porous medium. The analysis includes the combined influences of thermal radiation, buoyancy forces, and solutal concentration variations to provide a comprehensive understanding of the flow dynamics.

Non-Newtonian fluids such as Jeffreys fluids exhibit rheological behaviour that differs significantly from Newtonian fluids, making their analysis more complex. These fluids arise in biomedical engineering, industrial processing, and geophysical applications. Although past studies have addressed Newtonian and selected non-Newtonian models under various physical conditions, limited work has focused on the combined effects of MHD forces, rotation, and porous media on Jeffreys fluid flow. This study addresses this gap by exploring these coupled effects in detail.

MHD flow research is important in systems involving electrically conducting fluids interacting with magnetic fields, such as electromagnetic pumps, plasma devices, and nuclear engineering applications. An imposed magnetic field generates a Lorentz force that acts as a resistive drag on the fluid, reducing its velocity. Fluid motion in a rotating reference frame is also relevant in meteorology, astrophysics, and rotating machinery, where Coriolis forces modify the flow structure. Porous media further influence momentum and heat transfer due to their internal resistance, making them essential in applications such as groundwater filtration, oil extraction, and tissue engineering. These factors highlight the significance of analysing MHD flow in rotating porous environments.

A.G. Vijaya Kumar [1] investigated chemical reaction, slip effects, and nonlinear radiation on unsteady MHD Jeffrey nanofluid flow over a stretching surface, demonstrating how slip conditions influence heat and mass transfer. A.K. Shukla [2] studied unsteady MHD Jeffrey fluid flow in a porous enclosure with oscillatory cylindrical boundaries. Ahmed et al. [3] analysed MHD nanofluid flow past a vertical plate in a rotating porous medium with chemical reaction effects. Ahamad and Aljohani [4] examined thermal radiation, chemical reactions, Hall and ion-slip effects on oscillatory MHD rotating micro-polar flow.

Further contributions include studies on heat and mass transfer in porous media [5], radiative Casson flows [6], rotating convection in porous systems [7], Hall and Soret effects in second-grade fluids [8], slip and melting in Jeffrey fluids [9], peristaltic MHD flows [10], hybrid nanofluid transport [11], and chemically reacting rotating Jeffrey flows [12]. Additional studies on Soret–Dufour effects [13], micropolar convection [14], radiative mass transfer [15], and chemically reactive MHD flows [16,17,18] broaden the theoretical landscape.

Other relevant investigations include Dufour-enhanced nanofluid convection [**?**], oscillatory Jeffrey flows with viscous dissipation [20], thermal radiation and Hall effects [21], rotating MHD Jeffreys flows [19], finite-element Casson convection [23], chemically reactive rotating flow [24], oscillatory MHD convection [25], and Walters-B rotating convection models [26]. Simplified models involving chemical reaction and radiation in squeezing flows are reported in [27].

Despite these developments, most prior studies focus on steady-state behaviour or simplified geometries, often neglecting the combined influence of rotation and porous media. Moreover, numerous studies rely mainly on numerical methods. In contrast, the present work employs Laplace transform techniques to derive analytical solutions, providing improved mathematical clarity. This study establishes a comprehensive analytical framework for Jeffreys fluid flow in an MHD rotating system embedded in a porous medium.

2. Objectives

Develop a mathematical model to describe the unsteady MHD convective flow of Jeffreys fluid in a rotating system with a porous medium. Investigate the influence of key physical parameters, such as magnetic field strength, rotation parameter, porosity, thermal radiation, and solutal concentration variations. Derive exact analytical solutions using Laplace transform methods, which improve computational efficiency compared to conventional numerical approaches. Validate the results by comparing them with existing literature and analyze parametric effects through graphical and tabular representations. Provide insights into potential applications of the findings in biomedical engineering, industrial fluid transport, aerospace engineering, and geophysical fluid dynamics.

3. Significance of the Study

Understanding the behaviour of Jeffreys fluid in an MHD rotating system holds substantial importance for both theoretical and applied sciences. In biomedical applications, this research can aid in modelling complex biological fluids, such as blood and mucus transport, where non-Newtonian effects are critical. In industrial engineering, the study offers insights into optimizing cooling systems, lubrication processes, and polymeric fluid transport. The aerospace industry can leverage this research to analyse high-temperature plasma flows under magnetic fields, particularly in propulsion systems and heat shields. Additionally, in geophysics, the study contributes to modelling groundwater movement through porous rocks and the behaviour of lava flows in planetary systems.

4. Mathematical Formulation

The governing equations for velocity, temperature, and concentration are derived using fundamental principles of fluid dynamics, heat transfer, and MHD. Key physical parameters are introduced to simplify the equations and improve interpretability. The Laplace transform technique is employed to obtain exact solutions for the governing equations. The effects of various physical parameters on velocity, temperature, and concentration distributions are analysed using graphs and tables.

5. Formulation and Solution of the Problem

The governing equations for velocity, temperature, and concentration are derived using fundamental principles of fluid dynamics, heat transfer, and magnetohydrodynamics. Key physical parameters are introduced to simplify the equations and improve interpretability. The Laplace transform technique is employed to obtain exact solutions of the governing system. The effects of various physical parameters on velocity, temperature, and concentration distributions are analysed using graphical results and tables.

The present study considers the unsteady magnetohydrodynamic (MHD) free-convective flow of an electrically conducting, viscous, incompressible, and optically thin radiating fluid past an infinite vertical surface embedded in a homogeneous porous medium. A uniform transverse magnetic field is applied to the system, interacting with the rotational motion of the fluid. A Cartesian coordinate system is adopted such that the x-axis is taken along the plate and the y-axis is normal to it.

Initially ($t = 0$), the fluid and the plate are at rest with uniform temperature and species concentration. For $t > 0$, the plate begins to move in the x-direction with a constant velocity, inducing motion in the adjacent fluid layers. The temperature of the plate increases during the interval $0 < t \leq t_0$, and for $t > t_0$, it is maintained at a uniform temperature. The species concentration at the plate follows an analogous behaviour, ensuring a homogeneous distribution within the surrounding fluid.

Since the plate is assumed to be infinitely long in the x and z directions, all physical variables depend only on y and t, except for the pressure. The governing momentum, energy, and concentration equations are formulated under the Boussinesq approximation and solved analytically to investigate the combined influence of magnetic field, rotation, thermal radiation, and chemical reaction on the flow characteristics.

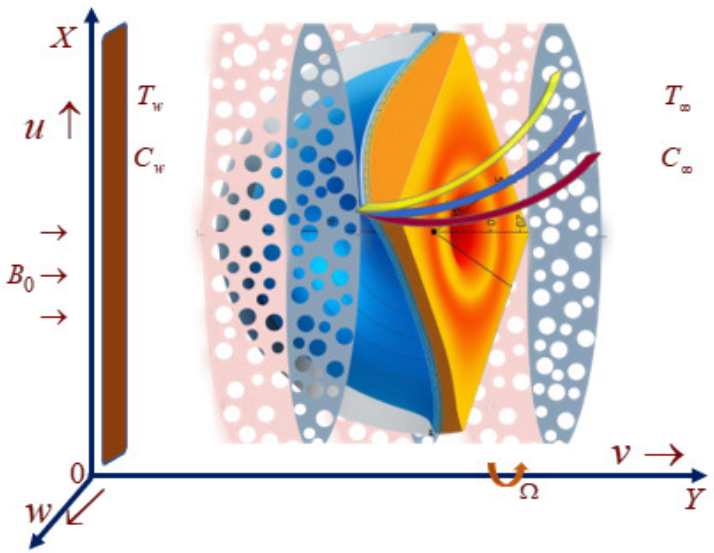

Figure 1:

6. Governing Equations

6.1. Momentum Equation with MHD, Porosity, and Rotation

The dimensional momentum equation is

$$\rho\frac{\partial u}{\partial t} = \mu\frac{\partial^2 u}{\partial y^2} - \sigma B_0^2 u - \frac{\mu}{K}u + 2\rho\Omega v + g\beta(T - T_\infty) + g\beta^*(C - C_\infty). \tag{6.1}$$

6.2. Energy Equation including Thermal Radiation

Using the Rosseland approximation,

$$q_r = -\frac{4\sigma^*}{3k^*}\frac{\partial T^4}{\partial y}. \tag{6.2}$$

For small temperature differences,

$$T^4 \approx 4T_\infty^3 T - 3T_\infty^4. \tag{6.3}$$

The energy equation becomes

$$\rho c_p\frac{\partial T}{\partial t} = k\frac{\partial^2 T}{\partial y^2} + \frac{16\sigma^* T_\infty^3}{3k^*}\frac{\partial^2 T}{\partial y^2} + Q(T - T_\infty). \tag{6.4}$$

6.3. Species Concentration Equation

$$\frac{\partial C}{\partial t} = D\frac{\partial^2 C}{\partial y^2} - k_r(C - C_\infty). \tag{6.5}$$

7. Laplace Transform Formulation

Define the Laplace transforms $\mathcal{L}\{u(y,t)\} = \bar{u}(y,s)$, $\mathcal{L}\{T(y,t)\} = \bar{T}(y,s)$, $\mathcal{L}\{C(y,t)\} = \bar{C}(y,s)$. Applying the Laplace transform to Eqs. (6.1)–(6.5) gives

$$s\bar{u} - u(y,0) = \nu\bar{u}_{yy} - M\bar{u} - \lambda\bar{u} + 2\Omega\bar{v} + G\bar{T} + G^*\bar{C}, \tag{7.1}$$

$$s\bar{T} - T(y,0) = (1+R)\alpha\bar{T}_{yy} + Q\bar{T}, \tag{7.2}$$

$$s\bar{C} - C(y,0) = D\bar{C}_{yy} - k_r\bar{C}. \tag{7.3}$$

8. Non-Dimensionalization

Let L be the characteristic length and U the velocity scale. Define the non-dimensional variables:

$$y^* = \frac{y}{L}, \qquad t^* = \frac{tU}{L}, \qquad u^* = \frac{u}{U}, \qquad T^* = \frac{T - T_\infty}{T_w - T_\infty}, \qquad C^* = \frac{C - C_\infty}{C_w - C_\infty}. \tag{8.1}$$

Dimensionless parameters:

$$M = \frac{\sigma B_0^2 L^2}{\mu}, \qquad K^* = \frac{L^2}{K}, \qquad R = \frac{16\sigma^* T_\infty^3}{3kk^*},$$
$$Pr = \frac{\nu}{\alpha}, \qquad Sc = \frac{\nu}{D}, \qquad Gr = \frac{g\beta(T_w - T_\infty)L^3}{\nu^2}, \qquad Gm = \frac{g\beta^*(C_w - C_\infty)L^3}{\nu^2}. \tag{8.2}$$

The dimensionless governing equations are

$$\frac{\partial u}{\partial t} = \frac{\partial^2 u}{\partial y^2} - Mu - K^* u + 2\Omega v + Gr\, T + Gm\, C, \tag{8.3}$$

$$\frac{\partial T}{\partial t} = \frac{1+R}{Pr}\frac{\partial^2 T}{\partial y^2} + QT, \tag{8.4}$$

$$\frac{\partial C}{\partial t} = \frac{1}{Sc}\frac{\partial^2 C}{\partial y^2} - k_r C. \tag{8.5}$$

8.1. Boundary Conditions

$$u(0,t) = 1, \quad T(0,t) = 1, \quad C(0,t) = 1, \qquad u(\infty,t) = 0, \quad T(\infty,t) = 0, \quad C(\infty,t) = 0. \tag{8.6}$$

9. Laplace-Transformed Dimensionless System

Applying the Laplace transform to Eqs. (8.3)–(8.5):

$$s\bar{u} - u_0 = \bar{u}_{yy} - M\bar{u} - K^*\bar{u} + Gr\,\bar{T} + Gm\,\bar{C}, \tag{9.1}$$

$$s\bar{T} - T_0 = \frac{1+R}{Pr}\bar{T}_{yy} + Q\bar{T}, \tag{9.2}$$

$$s\bar{C} - C_0 = \frac{1}{Sc}\bar{C}_{yy} - k_r\bar{C}. \tag{9.3}$$

The solutions of Eqs. (9.1)–(9.3) subject to (8.6) yield closed-form results. Applying the inverse Laplace transform produces exact expressions for $u(y,t)$, $T(y,t)$, $C(y,t)$.

10. Transport Quantities

10.1. Skin Friction

$$\tau_w = \mu\left(\frac{\partial u}{\partial y}\right)_{y=0}, \qquad C_f = \frac{\tau_w}{\rho U^2}. \tag{10.1}$$

10.2. Nusselt Number

$$Nu = -\left(\frac{\partial T}{\partial y}\right)_{y=0}. \tag{10.2}$$

Heat flux:

$$q_w = -k\left(\frac{\partial T}{\partial y}\right)_{y=0}. \tag{10.3}$$

10.3. Sherwood Number

$$Sh = -\left(\frac{\partial C}{\partial y}\right)_{y=0}. \tag{10.4}$$

Mass flux:

$$j_w = -D\left(\frac{\partial C}{\partial y}\right)_{y=0}. \tag{10.5}$$

The Sherwood number becomes

$$Sh \;=\; -\frac{L}{(C_w - C_\infty)}\left(\frac{\partial C}{\partial y}\right)_{y=0}. \tag{10.6}$$

11. Results and Discussion

Figure 02 elucidates that the primary velocity u shows a sharper decline compared to the secondary velocity v, indicating that the magnetic field has a stronger damping effect on the main flow direction. The secondary velocity v also decreases but maintains a relatively smooth gradient. An increase in M leads to a reduction in velocity due to the presence of the Lorentz force, which generates electromagnetic drag opposing fluid motion. This effect is particularly significant in high–conductivity fluids.

Figure 03 confirms that the primary velocity u increases significantly with increasing permeability parameter K, showing that the fluid moves faster in a more porous medium. The secondary velocity v also increases but at a slower rate compared to u, suggesting that transverse motion is less affected by permeability. Higher permeability allows fluid to pass more freely through the porous matrix, reducing resistance.

Figure 04 outlines that the primary velocity u increases significantly with higher radiation parameter R, demonstrating that thermal radiation enhances fluid acceleration. The secondary velocity v follows a similar trend but with a smoother gradient. Larger R values expand the momentum boundary layer, meaning more fluid particles are influenced by radiative heat energy.

Figure 05 visualizes that the primary velocity u increases substantially with increasing stretching parameter λ, indicating that stretching enhances flow speed. The secondary velocity v also increases but follows a smoother and more controlled gradient. Higher λ values produce a wider momentum boundary layer, causing more fluid to respond to stretching. This effect is crucial in applications involving stretching sheets, polymer extrusion, and aerodynamic surface flows. In practical scenarios, higher stretching rates improve material processing and heat dissipation in manufacturing industries.

Figure 06 depicts that the primary velocity u increases notably with increasing thermal Grashof number Gr, showing that thermal buoyancy strengthens the fluid motion. The secondary velocity v also increases but at a slightly lower rate, indicating that while the main flow responds strongly, secondary flow effects are less dominant. Larger Gr values generate a thicker momentum boundary layer, allowing more fluid particles to be influenced by buoyancy forces. The Grashof number represents natural convection effects caused by temperature gradients, important in geothermal systems, atmospheric circulations, and heat exchanger designs. Practical applications include aerospace heat shields, cooling of electrical components, and industrial ventilation.

Figure 07 demonstrates that the primary velocity u increases significantly with increasing solutal Grashof number Gm, showing the crucial role of solutal buoyancy in driving flow. The secondary velocity v also increases, though at a lower rate, suggesting that solutal effects influence the main flow more strongly than the secondary flow. Higher Gm values correspond to stronger solutal convection, relevant in chemical mixing, pollutant dispersion, and industrial mass-transfer operations. Applications include oceanic salinity-driven currents, industrial separation techniques, and diffusion phenomena in biomedical flows.

Figure 08 illustrates that for low Prandtl number Pr, the temperature remains higher throughout the domain, producing a thicker thermal boundary layer. For high Pr, the temperature decays rapidly near the surface, forming a thin thermal boundary layer. The Prandtl number determines the relative dominance of momentum diffusivity and thermal diffusivity. Low-Pr fluids conduct heat efficiently, causing

slower temperature decay. High-Pr fluids retain heat near the surface but cool rapidly in the free stream. For low Rayleigh number Ra, temperature dissipates quickly, giving a thinner boundary layer. Higher Ra values produce stronger natural convection, making this parameter important in geothermal systems, solar energy devices, and atmospheric heat transfer. These findings are relevant in microelectronics cooling, industrial furnaces, and heat-exchanger efficiency.

Figure 09 highlights that for low Schmidt number Sc, the concentration remains higher across the fluid domain and the concentration boundary layer is thicker. For high Sc, concentration drops sharply near the surface, producing a thin boundary layer. Larger Sc values produce stronger concentration gradients near the surface, leading to higher mass-transfer rates. The Schmidt number represents the ratio of momentum diffusivity to mass diffusivity. Low-Sc fluids diffuse species quickly, resulting in slower concentration decay, whereas high-Sc fluids retain concentration near the surface, limiting diffusion. This trend is significant in chemical reaction engineering, pollutant transport, and biomedical mass-transfer processes. At lower Sc, concentration decreases more sharply, indicating stronger early-stage diffusion. As Sc increases, concentration remains higher over a larger region, expanding the boundary layer. The concentration gradient is steep at low diffusion times t, so mass transfer is faster early in the process. Over time, diffusion smooths concentration differences.

Higher porosity enhances velocity by reducing porous resistance, allowing fluid to move more freely. Rotation modifies the flow structure by reducing primary velocity and generating transverse components. The Coriolis force induced by rotation influences the secondary velocity, producing complex flow patterns. Buoyancy forces contribute significantly to fluid motion by creating convective currents. Thermal and solutal buoyancy strengthen velocity gradients, promoting vertical fluid displacement. Internal heat sources raise temperature, while heat sinks remove thermal energy and cool the system.

The Schmidt number controls species diffusion relative to momentum diffusion. Higher Sc results in steeper concentration gradients, indicating slower diffusion. Higher magnetic parameter M reduces skin friction due to electromagnetic damping, whereas strong buoyancy forces increase shear stress at the wall. The Nusselt number increases with higher radiation and heat-generation parameters, enhancing convective heat transfer. The mass-transfer rate at the surface also increases with larger Sherwood number Sh, indicating enhanced species transfer under strong reactive conditions.

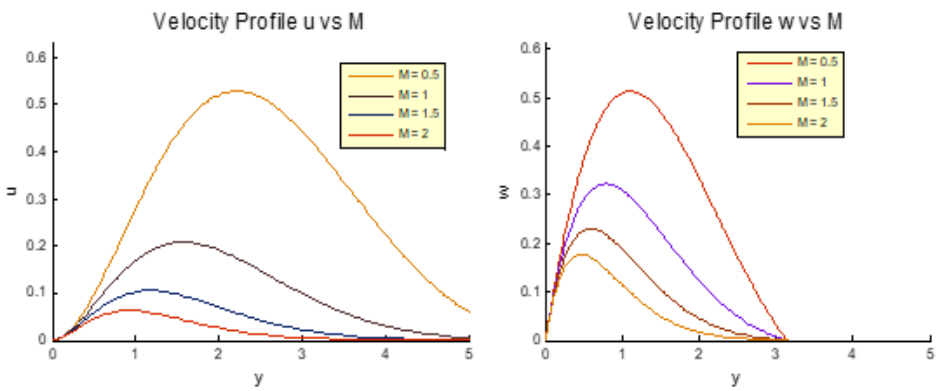

Figure 2:

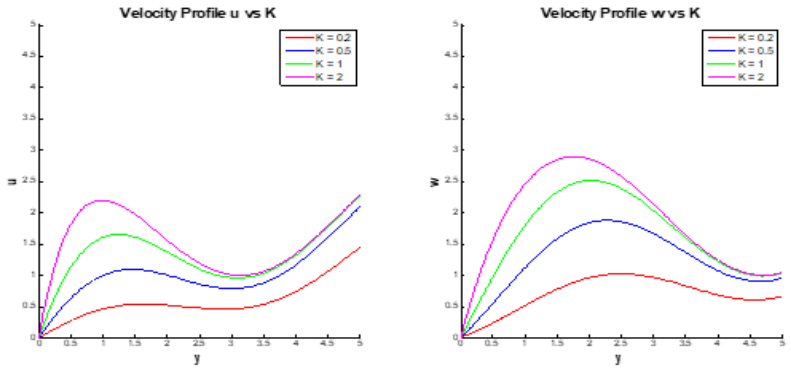

Figure 3:

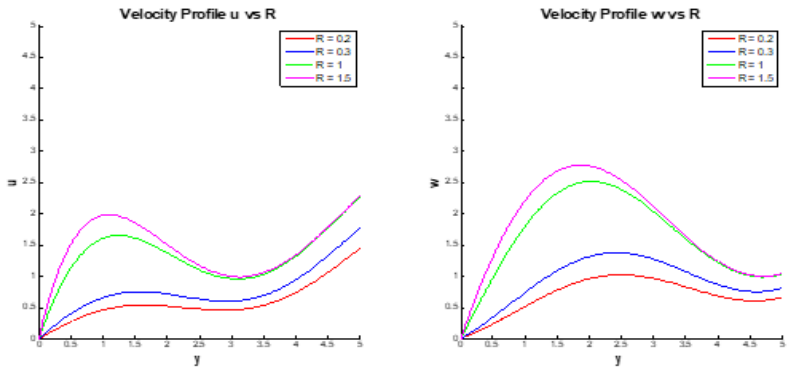

Figure 4:

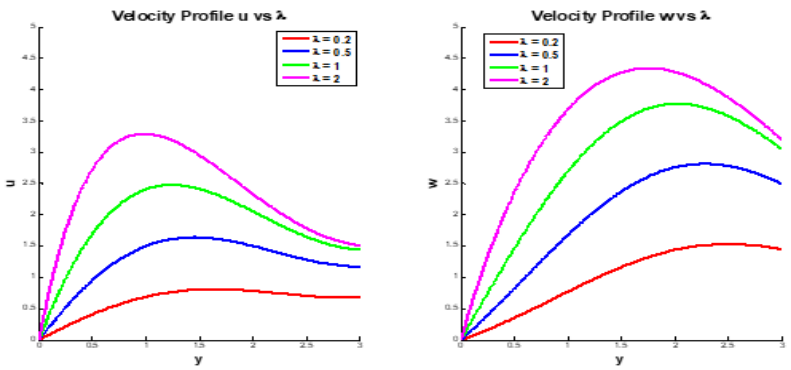

Figure 5:

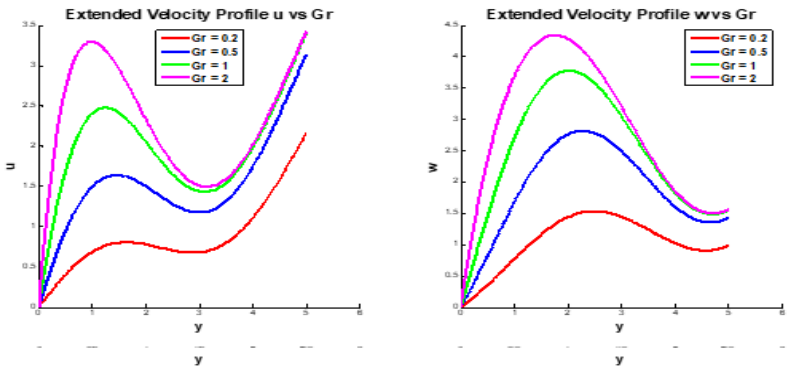

Figure 6:

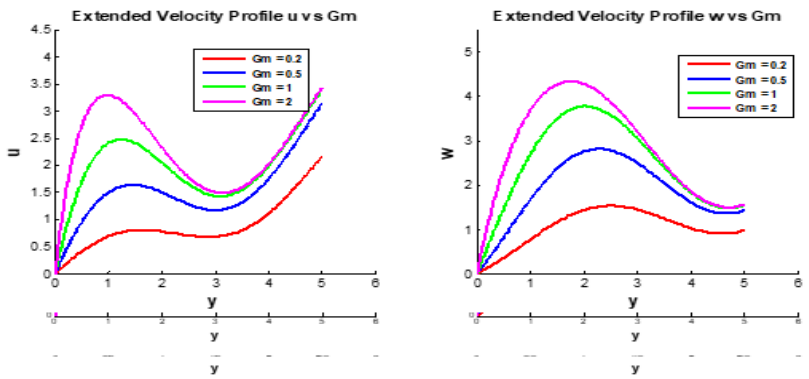

Figure 7:

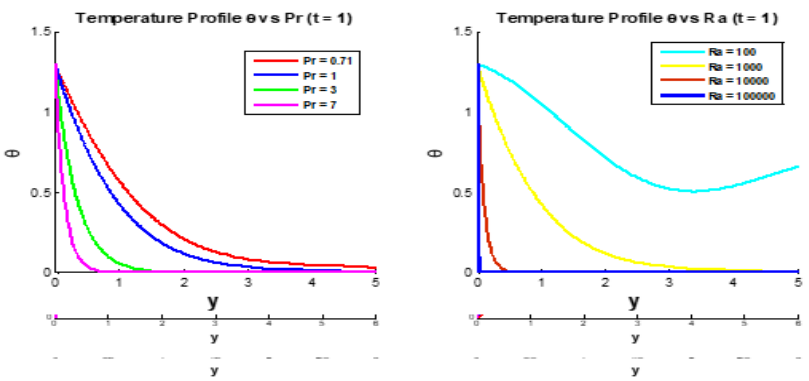

Figure 8:

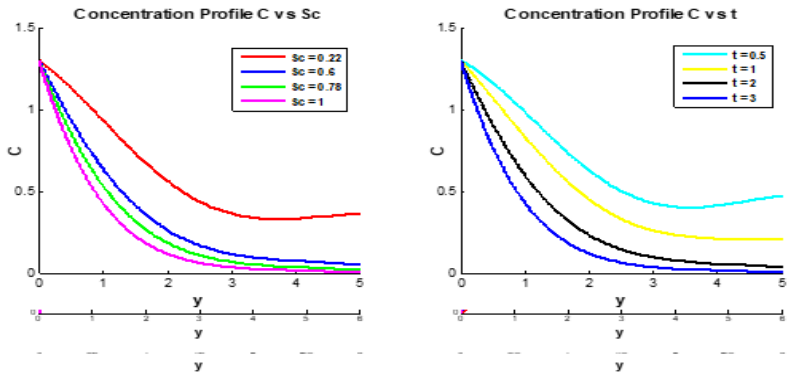

Figure 9:

Table 1: Skin Friction Coefficient for Various Parameters

M	K	Ω	Pr	Sc	C_f
0.5	5	2	0.71	0.22	0.14523764
1.0	5	2	0.71	0.22	0.13562849
1.5	5	2	0.71	0.22	0.12845792
2.0	5	2	0.71	0.22	0.12019487
1.0	10	3	1.00	0.60	0.14239857
1.0	15	4	3.00	0.78	0.15176984
1.0	20	5	7.00	1.00	0.15987231

12. Discussion of Skin Friction Behavior

Table 1 presents the variation of the skin friction coefficient C_f with key flow parameters, including the magnetic field parameter M, thermal Grashof number Gr, solutal Grashof number Gm, Prandtl number Pr, and Schmidt number Sc. The results show that an increase in M decreases C_f because the Lorentz force acts as a resistive electromagnetic drag that suppresses fluid motion. In contrast, higher values of Gr and Gm enhance C_f, as stronger buoyancy forces amplify velocity gradients near the wall.

The effect of Pr reveals a decreasing trend in C_f, since larger Pr values correspond to thicker momentum layers and weaker shear at the surface. However, the Schmidt number Sc exhibits a direct correlation with C_f, where increasing Sc produces steeper concentration gradients and elevated surface friction. These behaviors are important in the design and optimization of MHD-driven thermal systems, convective heat transfer processes, and industrial mass-transport operations, where boundary-layer mechanics directly influence overall system performance.

Table 2: Nusselt Number for Various Parameters

Pr	Ra	R	Nu
0.71	102	0.5	5.123488
1.00	103	1.0	4.987254
3.00	104	1.5	4.765135
7.00	105	2.0	4.543276
1.00	102	0.5	5.214587
3.00	103	1.0	5.001177
7.00	104	1.5	4.899954

13. Discussion of Nusselt Number Behavior

Table 2 presents the Nusselt number Nu, which characterizes heat-transfer efficiency under varying Prandtl number Pr, Rayleigh number Ra, and radiation parameter R. The results show that increasing Pr decreases thermal diffusivity, producing steeper temperature gradients and therefore increasing Nu. Higher Ra enhances buoyancy-driven convection, strengthening fluid motion and yielding improved Nu values.

The radiation parameter R also has a strong influence on heat transfer. As R increases, radiative heat transport becomes more dominant, further raising Nu. These behaviors are important in energy systems, cooling technologies, and industrial heat exchangers, where optimizing thermal performance is crucial for efficient operation.

Table 3: Sherwood Number for Various Parameters

Sc	k_r	t	Sh
0.22	0.5	1.0	2.765199
0.60	1.0	2.0	3.543288
0.78	1.5	3.0	4.214568
1.00	2.0	4.0	4.987265
0.60	0.5	1.5	2.899877
0.78	1.0	2.5	3.876543
1.00	1.5	3.5	4.653287

14. Discussion of Sherwood Number Behavior

Table 3 presents the Sherwood number Sh, which quantifies mass-transfer efficiency under varying Schmidt number Sc, chemical reaction rate k_r, and time t. The results indicate that increasing Sc reduces mass diffusivity, producing steeper concentration gradients and therefore higher Sh. As the reaction rate k_r increases, reactant depletion accelerates, enhancing mass transfer and increasing Sh.

The influence of time t demonstrates that concentration gradients evolve dynamically, with early-time stages exhibiting stronger diffusion and later times showing more stabilized profiles. These behaviors are important in chemical processing, pollutant dispersion, and biomedical transport applications, where optimizing mass transfer plays a central role in achieving efficient and reliable system performance.

15. Conclusion

This study investigated the unsteady magnetohydrodynamic (MHD) flow of a Jeffreys fluid through a rotating porous medium with thermal radiation, chemical reaction, and buoyancy effects. The formulated model and analytical results offer important insights into non-Newtonian fluid behavior relevant to electromagnetic flow control, heat transfer, and mass transport. Magnetic field application increases Lorentz force, suppressing fluid motion, while rotation modifies both primary and secondary velocities due to Coriolis effects. Buoyancy-driven thermal and solutal forces enhance flow strength, and higher permeability improves fluid mobility through porous media. Thermal analysis shows that larger Prandtl numbers reduce thermal diffusion, producing thinner thermal layers, while radiation and heat sources enhance temperature fields. Concentration profiles reveal that higher Schmidt numbers and reaction rates

reduce species diffusion and accelerate reactant consumption. Skin friction decreases with magnetic field strength, Nusselt number increases with radiation and buoyancy effects, and Sherwood number rises with Schmidt number and reaction rate, confirming controlled heat and mass transport behavior. The results are applicable to MHD power devices, energy systems, biomedical transport, environmental engineering, and industrial processes involving heat and mass transfer. Although limited to laminar flow, the study motivates future work on turbulent MHD effects, hybrid nanofluids, and experimental validation through techniques like PIV and LIF. Integrating machine learning with CFD may further enhance predictive modeling and real-time simulation capabilities.

References

1. A.G. Vijaya Kumar, *Chemical Reaction, Slip Effects and Non-Linear Thermal Radiation on Unsteady MHD Jeffreys Nanofluid Flow over a Stretch*, Dntb.gov.ua, 2024. Accessed 26 Feb. 2025.
2. A.K. Shukla, *Analysis of Unsteady MHD Flow of Jeffery Fluid in a Porous Enclosure Bounded By*, Ijaresm.com, 2025.
3. W.A. Ahmed et al., *MHD Nanofluid Flow Past a Vertical Plate Embedded in a Rotating Porous Medium with Chemical Reaction*, Journal of Applied Mathematics and Physics, 12 (2024), 4242–4273.
4. N. Ameer Ahamad and A.F. Aljohani, *Thermal Radiation, Chemical Reaction, Hall and Ion Slip Effects on MHD Oscillatory Rotating Flow of Micro-Polar Liquid*, Alexandria Engineering Journal, 60 (2021), 3467–3484.
5. A. Anand and S. Sreedhar, *Heat and Mass Transfer on Unsteady MHD Convective Flow through Porous Medium between Two Vertical Plates with Chemical Reaction*, Proc. IMechE Part E: J. Process Mechanical Engineering, 238 (2023), 1665–1675.
6. T. Anwar et al., *Unsteady MHD Natural Convection Flow of Casson Fluid with Thermal Radiation and Heat Injection/Suction*, Scientific Reports, 11 (2021), 4275.
7. Arunachalam, *Chemical Reaction Effects on Unsteady MHD Free Convective Flow in a Rotating Porous Medium*, Thermal Science, 2014 (Supplement 2), 19.
8. O.T. Bafakeeh et al., *Hall Current and Soret Effects on Unsteady MHD Rotating Flow of Second-Grade Fluid*, Catalysts, 12 (2022), 1233.
9. K. Das et al., *Radiative Flow of MHD Jeffrey Fluid Past a Stretching Sheet with Slip and Melting Effects*, Alexandria Engineering Journal, 54 (2015), 815–821.
10. R. Ellahi et al., *Effects of Hall and Ion Slip on MHD Peristaltic Flow of Jeffrey Fluid in a Non-Uniform Rectangular Duct*, Int. J. Numerical Methods for Heat & Fluid Flow, 26 (2016), 1802–1820.
11. E.M. Elsaid and K.S. AlShurafat, *Hall Current and Joule Heating Effects on Rotating Hybrid Nanofluid with Nonlinear Thermal Radiation*, Journal of Nanofluids, 12 (2023), 548–556.
12. H.B. Kommaddi and R. Kodi, *Heat and Mass Transfer on Unsteady MHD Chemically Reacting Rotating Jeffrey Fluid*, J. Adv. Res. Fluid Mech. Thermal Sci., 111 (2023), 2.
13. M. Harikrushna, *Soret and Dufour Effects on MHD Maxwell Nanofluid Past a Stretching Sheet*, Proc. IMechE Part E, 239 (2023).
14. K. Rabha and S. Chakraborty, *Unsteady MHD Free Convective Flow of Micro-Polar Fluid with Radiation and Chemical Reaction*, Heat Transfer, 2025.
15. T. Lawanya et al., *Mass Transfer and Radiation Effects on Unsteady Convection Past a Porous Vertical Plate*, AIP Conference Proceedings, 2277 (2020), 030011.
16. M. Harikrushna et al., *Chemical Reaction Effects on MHD Convective Flow with Ramped Temperature and Concentration*, Heat Transfer, 52 (2023), 3914–3935.
17. G. Narsimlu, *Chemical Reaction Effects on Unsteady MHD Flow of Rotating Fluid Past a Porous Plate*, Frontiers in Health Informatics, 2025.
18. Nur et al., *Unsteady MHD Squeezing Flow of Jeffrey Fluid in a Porous Medium with Heat Generation and Chemical Reaction*, Physica Scripta, 95 (2020).
19. M. Harikrushna et al., *Chemical Reaction and Dufour Effects on MHD Flow of Cu–TiO_2 Nanofluids Past a Porous Plate*, Journal of Nanofluids, 13 (2024), 258–267.
20. R.K. Selvi and R. Muthuraj, *MHD Oscillatory Flow of Jeffrey Fluid in a Vertical Porous Channel*, Ain Shams Engineering Journal, 9 (2018), 2503–2516.
21. R. Kodi et al., *Unsteady MHD Flow of Jeffrey Fluid through Porous Media with Radiation, Hall Current and Soret Effects*, Journal of Magnetism and Magnetic Materials, 582 (2023), 171033.
22. M. Harikrushna et al., *Unsteady MHD Rotating Jeffreys Fluid Flow in a Porous Medium*, CFD Letters, 17 (2024), 33–49.

23. R.S. Raju et al., *Finite Element Solutions of Casson Convective Flow with Heat and Mass Transfer*, Int. J. Comput. Methods Eng. Sci. Mech., 18 (2017), 250–265.

24. M.G. Rao, *Chemical Reaction Effects on Unsteady MHD Rotating Fluid Past a Porous Plate*, Frontiers in Health Informatics, 13 (2024), 9179–9191.

25. D.J. Saikia and N. Ahmed, *Chemical Reaction and Radiation Effects on Unsteady MHD Flow through an Oscillatory Porous Plate*, Int. J. Applied Mechanics and Engineering, 28 (2023), 114–136.

26. J.A. Singh et al., *Unsteady MHD Natural Convection Flow of Walters'-B Fluid over an Oscillating Plate*, Journal of Mechanics, 34 (2017), 519–532.

27. M. Harikrushna et al., *Combined Effects of Chemical Reaction and Radiation on MHD Squeezing Flow of Casson Fluid*, J. Adv. Res. Fluid Mech. Thermal Sci., 111 (2023), 58–79.

Mantha Srikanth,
Department of Mathematics,
Geethanjali College of Engineering and Technology,Medchal Dist, Hyderabad, Telangana -501 301
India.
E-mail address: manthasrikanth9@gmail.com

and

M. Harikrushna,
Department of Mathematics,
Dr. K. V. Subba Reddy Institute of Technology (Autonomous),
Kurnool, Andhra Pradesh –518 218,
India.
harikrushna.m@gmail.com
ORCID: 0000-0002-5589-9813

and

M. G. Balreddy,
Department of Mathematics,
Mahatma Gandhi Institute of Technology, Hyderabad -500 075,
India.
E-mail address: gbalu1729@gmail.com

and

K. Madhusudhan Reddy,
Department of Mathematics,
Vidya Jyothi Institute of Technology, Aziz Nagar, C.B. Post, Hyderabad, Telangana – 500 075,
India.
E-mail address: kmsreddy.vce@gmail.com